frontiers | Frontiers in Earth Science

TYPE Original Research
PUBLISHED 24 February 2025
DOI 10.3389/feart.2025.1554436

OPEN ACCESS

EDITED BY
Liangcheng Tan,
Chinese Academy of Sciences (CAS), China

REVIEWED BY
Jiaju Zhao,
Chinese Academy of Sciences (CAS), China
Yanling Li,
Yunnan University, China

*CORRESPONDENCE
Dejun Wan,
dejunwan@ntu.edu.cn

RECEIVED 02 January 2025
ACCEPTED 03 February 2025
PUBLISHED 24 February 2025

CITATION
Ning D, Sun W, Wan D, Cheng L and Jiang Q (2025) Late Holocene Indian summer monsoon evolution and centennial fluctuations inferred by grain-size sensitive component from Lake MangCo, southeastern Tibetan Plateau.
Front. Earth Sci. 13:1554436.
doi: 10.3389/feart.2025.1554436

Late Holocene Indian summer monsoon evolution and centennial fluctuations inferred by grain-size sensitive component from Lake MangCo, southeastern Tibetan Plateau

Dongliang Ning[1], Weiwei Sun[2], Dejun Wan[1]*, Longjuan Cheng[1] and Qingfeng Jiang[1]

[1]School of Geographic Science, Nantong University, Nantong, China, [2]State Key Laboratory of Lake Science and Environment, Nanjing Institute of Geography and Limnology, Chinese Academy of Sciences, Nanjing, China

Identifying the late Holocene Indian summer monsoon (ISM) changes and their possible forcing mechanisms provides an important perspective for understanding the current monsoon shifts driven by anthropogenic climate change within a natural baseline. In this study, we present a well-dated, ca. 4.0 ka grain-size sensitive component record from Lake MangCo, located in the southeastern Tibetan Plateau. The record depicts late Holocene ISM evolution and centennial-scale precipitation events superimposed on millennial-scale climate changes. The results indicate that precipitation was relatively high during the first half of the late Holocene, likely before 2.0 cal ka BP, followed by a period of relatively reduced precipitation thereafter, which indicates that the Northern Hemisphere summer insolation (NHSI) has primarily controlled ISM intensity. A slight increasing trend in ISM strength since 1.1 cal ka BP was observed, which may correspond to the reported "2.0-kyr-shift" and could be related to warming tropical temperatures. Three low precipitation intervals, occurring at ~1.1, 2.0, and 3.2 cal ka BP, align well with known centennial-scale ISM weakening events during the late Holocene, such as the Medieval Warm Period (MWP) and the "2.0-ka-dry-event." Our findings further validate the climatic effects of tropical ocean–atmospheric interactions in the Pacific and Indian Ocean basins on ISM variabilities at centennial timescales.

KEYWORDS

late Holocene, Indian summer monsoon, centennial fluctuation, summer insolation, ENSO

1 Introduction

The Indian summer monsoon (ISM) is a crucial component of the global climate system, transporting moisture and heat from tropical oceans to higher-latitude continents (Overpeck et al., 1996). Changes in monsoonal precipitation can cause extreme floods and droughts, which has far-reaching impacts on regional economies and social stability, particularly in ISM-influenced areas, which are home to more than half of the world's

population (Verma et al., 2022). During the past few decades, the effects of human-induced greenhouse gas emissions seem to have significantly changed the natural ISM trajectory with increasing frequencies and magnitudes in extreme monsoonal precipitation events (Jiang Y. et al., 2023; Katzenberger et al., 2021). However, limited by the temporal spans of the instrumental observation results, the relative contribution of anthropogenic and natural effects can hardly be separated (Hansen and Stone, 2016). Therefore, identifying paleo-ISM dynamics over longer timescales, along with their underlying mechanisms, is particularly important for informing present and future socio-economic policymaking in the context of global warming.

The late Holocene period provides valuable insights into the long-term evolution of the ISM, which helps contextualize current shifts in the monsoon system driven by anthropogenic climate change. Evidence from high-resolution stalagmite oxygen isotope ($\delta^{18}O_{stallagmite}$) records (Dutt et al., 2021; Fleitmann et al., 2007; Zhang et al., 2008), marine sediments (Anderson et al., 2010; Conroy et al., 2008; Huguet et al., 2006), and lacustrine and peatland deposits (Cui et al., 2022; Ming et al., 2020; Wang J. et al., 2024) illustrated that the ISM varied considerably during the late Holocene. However, there are strong discrepancies and temporal–spatial heterogeneity between various paleoclimate records. For example, previous studies have found a generally decreasing trend in the ISM intensity during the late Holocene that may be closely related to the gradual decline of Northern Hemisphere summer insolation (NHSI) (Bird et al., 2017; Hong et al., 2003; Prasad et al., 2014). However, emerging evidence demonstrates that the ISM might have experienced a strengthening trend after approximately 2.0 cal ka BP, which is distinctly divergent from the expected response based on insolation changes alone (Ming et al., 2020; Wang J. et al., 2024). Such a phenomenon has been proposed as the "2-kyr-shift," which might have resulted from the enhancement of Atlantic Meridional Overturning Circulation (AMOC) (Cheng et al., 2016) or the strengthened feedback of higher greenhouse gas concentrations (Ming et al., 2020). On centennial timescales, the ISM exhibited significant fluctuations during the late Holocene, but the nature of the regional climate shift, characterized by whether "warm-dry and cold-wet" conditions or the opposite, remains controversial, especially for the typical periods like the Medieval Warm Period (MWP) and Little Ice Age (LIA) (Chen et al., 2015; Xu et al., 2017). Various paleoclimate results have attributed centennial-scale ISM oscillations to multiple factors, including the variability in solar forcing (Gupta et al., 2005; Tiwari et al., 2015), surface temperature variations in the Atlantic Ocean (Zhang et al., 2016), and sea surface temperature (SST) anomalies in the Indian and Pacific oceans (Ming et al., 2020; Sun et al., 2023). Clearly, further crucial evidence from monsoonal regions is required to improve our understanding of the ISM system and possible forcing mechanisms.

The southeastern Tibetan Plateau (TP) is highly sensitive to global climate change and strongly influenced by the ISM (An et al., 2015). High-elevation mountain lakes in this region can preserve high-resolution records of environmental changes with minimal anthropogenic impact, ensuring more accurate reconstructions of natural climate variability. In this study, we present a well-dated paleoclimate record based on sediment grain-size analyses from Lake MangCo, spanning the last four millennia, to investigate the late Holocene monsoonal precipitation changes. We further compared our results with regional paleoclimate records and SST changes to explore the possible interactions between ISM fluctuation and the tropical ocean–atmospheric coupling system.

2 Materials and methods

2.1 Study site

Lake MangCo (29°34′N, 98°51′E, 4,310 m a.s.l.) is located in the Mangkang County, southeastern Tibetan Plateau. It is a tectonic lake with a maximum water depth of 22.8 m. The lake surface area is approximately 21 km^2, and the catchment area is approximately 110 km^2. There are no glaciers in the high-altitude catchment areas, which indicates that it is hydrologically recharged by precipitation, surface runoff, and the perennial inflow from the northern mountain valley (Huang et al., 2025). There is a single outflow river located in the northeastern part of the lake, situated close to the inflow river, which ultimately flows into the Jinsha River (Figure 1C). The climate in this area is strongly influenced by the ISM in summer and the southern branch of the westerlies in winter. The mean annual precipitation is 446 mm (between 1980 and 2010), most of which (80%) falls during the summer months of June through September (Huang et al., 2025). The annual mean air temperature in this region is approximately 2°C.

2.2 Coring and dating

A 101-cm-long sediment core was retrieved from the deepest part of the lake (approximately 22.5 m) using a UWITEC gravity corer in October 2022 (Figure 1). The sediment–water interface in the sediment core remained clear and undisturbed. The sediment core was then sub-sampled at 1-cm intervals and stored at 4°C prior to analysis.

The chronology of the sediment core is obtained by combining the dating results of radionuclides and radiocarbon ages. The upper sections were used to measure ^{210}Pb, ^{226}Ra, and ^{137}Cs activities using an ORTEC HPGe GWL series well-type coaxial low background intrinsic germanium detector. Gamma emissions were recorded at 46.5 keV for ^{210}Pb, at 295 keV for ^{226}Ra, and at 352 keV for ^{214}Pb, following 3 weeks of storage in a sealed container to allow radioactive equilibration, while ^{137}Cs activity was recorded at 662 keV (Appleby, 2001). The unsupported ^{210}Pb ($^{210}Pb_{ex}$) in each sample was obtained by subtracting the activity of ^{226}Ra from the total activity of ^{210}Pb. The absolute efficiency of the detector was determined using calibrated sources and samples of known activity. Corrections were made for the effect of self-absorption of low-energy gamma rays within the sample (Appleby, 2001). Four plant materials were submitted to the Beta Analytic Radiocarbon Dating Laboratory (United States) for accelerator mass spectrometry (AMS) ^{14}C dating. The AMS ^{14}C dates were calibrated to calendar years before the present (0 BP = 1950 CE) using the IntCal20 calibration dataset (Reimer et al., 2020). The final age–depth relationship is interpolated using a Bayesian model in the Bacon program (Blaauw and Christen, 2011) implemented in R 4.1.1 with default settings for lake sediments (R Development Core Team, 2013).

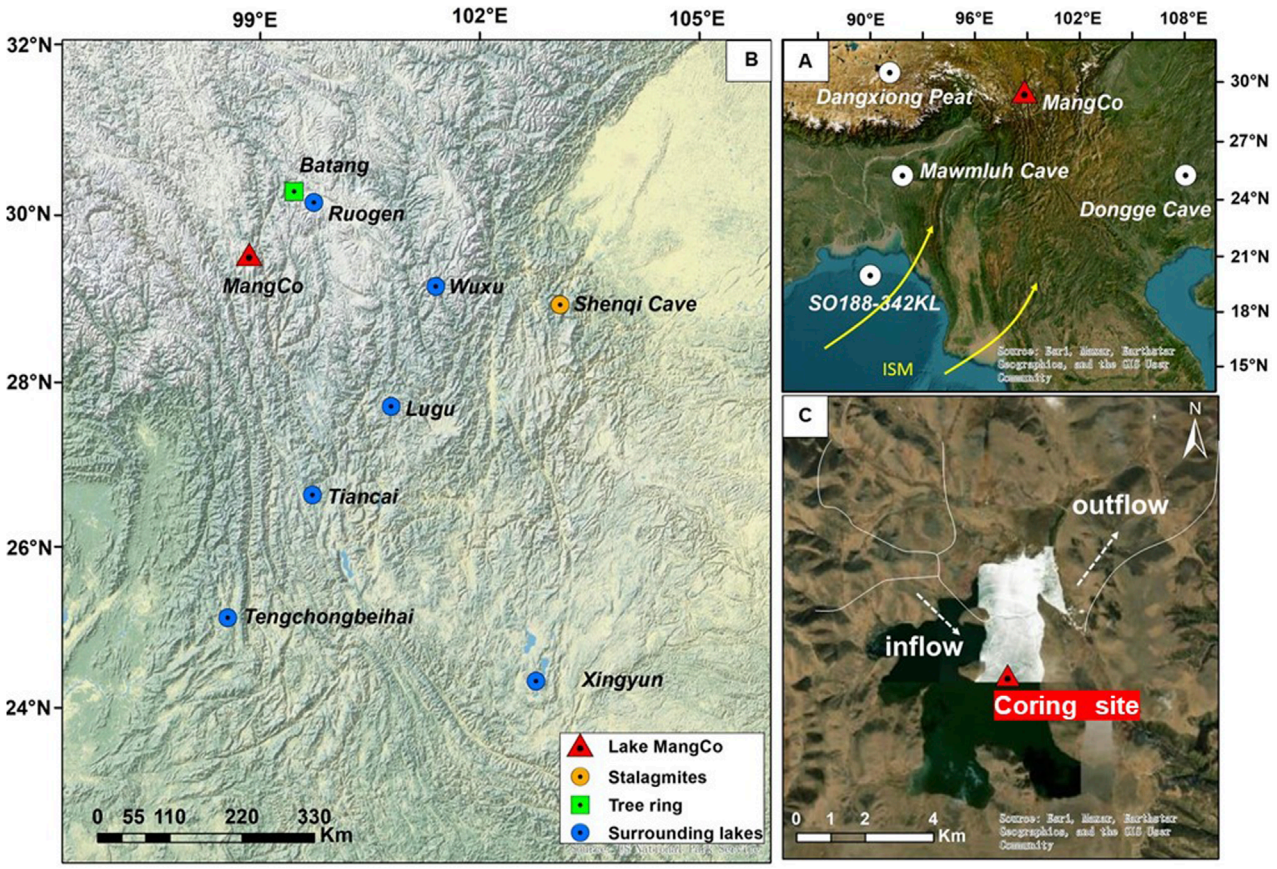

FIGURE 1
(A) Location of Lake MangCo (red triangle) and the surrounding paleoclimate records mentioned in this study including the Dongge Cave (Dykoski et al., 2005), the Mawmluh Cave (Dutt et al., 2021), the marine sediment from core SO188-342 KL (Contreras-Rosales et al., 2014), and Dangxiong peatland (Wang J. et al., 2024). **(B)** Adjacent records in southwestern China including lacustrine sediments from Lake Ruogen (Ming et al., 2020), Lake Wuxu (Zhang et al., 2016), Lake Lugu (Sheng et al., 2015), Lake Tiancai (Xiao et al., 2014), Lake Tengchong Beihai (Wang et al., 2020), and Lake Xingyun (Chen et al., 2015); tree-ring records from Bangtang (An et al., 2013) and stalagmite record from the Shenqi Cave (Tan et al., 2018). **(C)** The coring site and the catchment landscape of Lake MangCo; the white lines indicate the rivers in the surrounding areas.

2.3 Grain-size analyses

Grain size was measured at every 1-cm interval on wet sediment using the Malvern® Mastersizer 2000 Laser Particle size Analyzer (detection size range: 0.02–2000 μm). Before measurement, H_2O_2 and HCl were added to samplers to remove organic carbon and carbonate. The pretreated samples were dispersed using $(NaPO_3)_6$ in an ultrasonic bath for 15 min. All the samples were measured three times, and a final average value was assigned to each sample to reduce test error. The grain size vs. standard deviation method was chosen to identify the sensitive grain size classes with higher standard deviations (Sun et al., 2003).

3 Results

3.1 Chronology

The $^{210}Pb_{total}$ activity reached an equilibrium value at 20 cm but is greater than ^{226}Ra activity (Figure 2A), which might be related to the efficiency calibration error with the gamma spectrometers. A correction value was calculated by subtracting the mean supported ^{226}Ra activity from the mean asymptotic activity of $^{210}Pb_{total}$ at the bottom samples below 20 cm. The corrected $^{210}Pb_{ex}$ activity was obtained by subtracting the correction value from the original $^{210}Pb_{ex}$ activity at each level (Figure 2B). A distinct peak in ^{137}Cs activity at a depth of 8 cm was identified, corresponding to the peak atmospheric ^{137}Cs fallout from nuclear weapon testing in 1963 CE (Figure 2B). Considering the compaction effect, we used the ^{137}Cs-corrected constant rate of supply (CRS) model to establish the chronology in the upper 20-cm sediments (Figure 2C).

Radiocarbon ages are presented in Table 1, and the final age–depth model of the whole sediment core is plotted in Figure 3. The ^{13}C value of the dating material at 10 cm intervals is −14.2‰, which indicates that this sample might be retrieved from the macrophyte plants and the possible ^{14}C reservoir effect should be considered. Therefore, we abandon this result in the final chronology. Using the three other ^{14}C dating results, we obtained a deposition rate of 0.025 cm under natural background. Those results lead to an equilibrium of ^{210}Pb activity at 20 cm, which is the

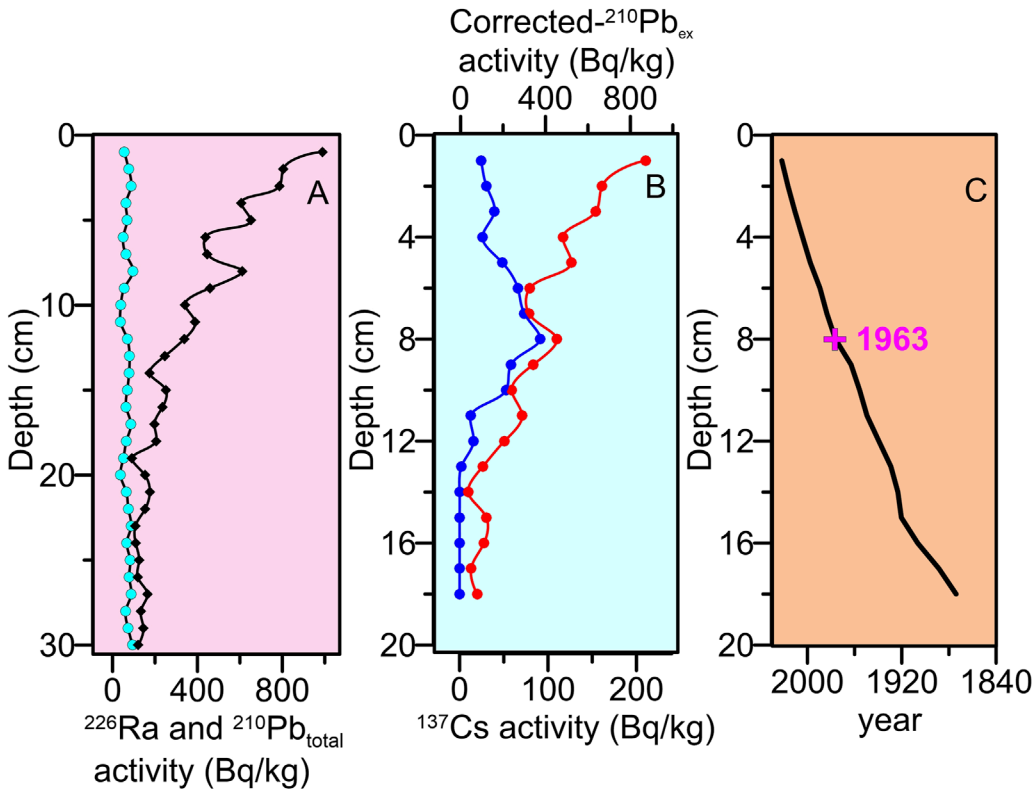

FIGURE 2
Dating results of the upper section from Lake MangCo. **(A)** ^{226}Ra (cyan circle) and $^{210}Pb_{total}$ (black diamond) activity, **(B)** ^{137}Cs (blue line) and corrected-$^{210}Pb_{ex}$ (red line) activity, and **(C)** ^{137}Cs-corrected CRS dating results.

TABLE 1 AMS radiocarbon dates from Lake MangCo.

Laboratory number	Sample depth/cm	$\delta^{13}C$/‰	^{14}C age/±30 years	Calibrated age/2σ	Median age/cal year BP
BETA607405	10	−14.2	630		
BETA624438	42	−22.5	1,210	1,039–1,298	1,168
BETA607407	75	−23.3	3,020	2,922–3,418	3,220
BETS607408	100	−22.1	3,500	3,647–4,027	3,863

same as the ^{210}Pb and ^{226}Ra results (Figure 2A). Therefore, the three other AMS ^{14}C could be directly used to establish the age–depth model with little old carbon effect. The final average basal age of the sediment core is ca. 3.8 cal ka BP.

3.2 Grain-size variation

The grain size probability curves display multimodal distributions (Figure 4A). The grain size standard deviation peaks at 0.7 μm, 4 μm, and 104 μm. However, we observed that peak 104 μm corresponds only to the grain-size distribution at 60 cm, which we attribute to measuring errors. Therefore, we identified two sensitive components based on the standard deviation peaks with the corresponding size range smaller and larger than 4 μm and designated them as SC1 and SC2, respectively. The SC2 abundance maintained a relatively higher content than that of SC1 with averages of 57.8% and 42.2%, respectively. The SC2 content was relatively high (61.7%) during the first half of the late Holocene, likely before 2.0 cal ka BP, except for a low period between 3.4 and 3.0 cal ka BP with a mean of 55.2%. After striking low content intervals centered at 2.0 cal ka BP, the SC2 content slightly increased but has never exceeded the mean values before 2.0 cal ka BP. The content of SC1 has varied inversely with that of SC2 throughout the core, which might indicate possible opposite impacts from the same climatic factors on the grain-size variations.

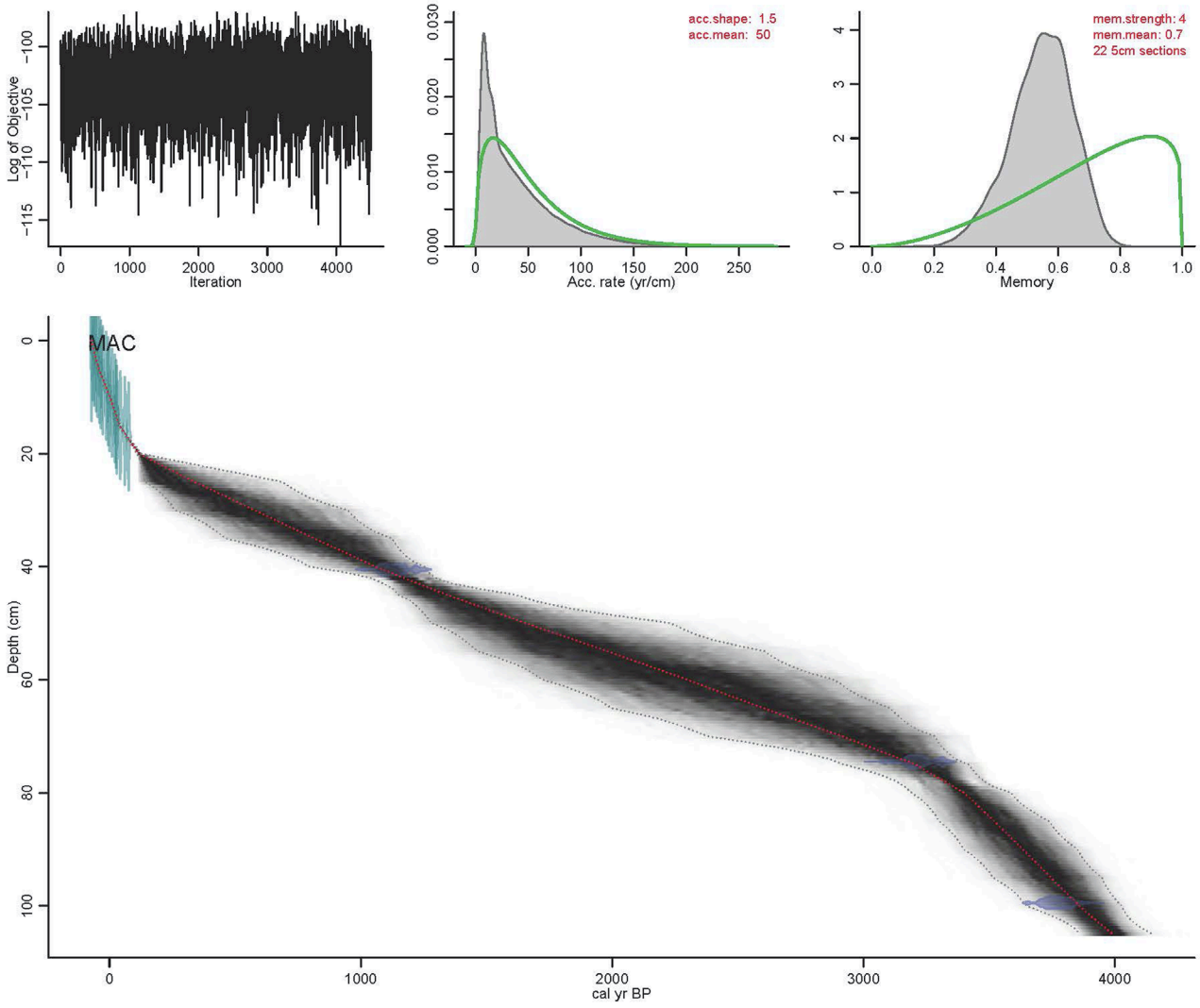

FIGURE 3
Age–depth model for the Lake MangCo sediment core produced using Bacon software (Blaauw and Christen, 2011). The dotted lines (gray) indicate the 95% confidence limits, and the dashed line (red) shows the weighted mean ages for each depth.

4 Discussion

4.1 Climatic interpretation of grain size in Lake MangCo

The grain-size distribution of the lake sediments offers valuable information referring to the changes in lake hydroclimatic conditions, which has been widely used in paleoclimate studies (Liu et al., 2016; Ming et al., 2020; Ning et al., 2024; Xiao et al., 2009). However, the deposition process of the particles could be influenced by various factors, including changes in transport dynamics, fluctuations in lake levels, and shifts in clastic material sources (Last and Smol, 2001). In our study, the relatively small catchment area limits the particle derivation in the surroundings. Therefore, the hydrodynamic condition in the lake basins is the primary factor influencing grain-size composition. It has been observed that there is usually a ring-shaped distribution of grain size in lake basins with fine grains increasing from the nearshore to the center due to the higher hydraulic energy in the nearshore shallow water zone than in offshore deeper areas (Last and Smol, 2001). Therefore, water level decrease (increase) during extreme dry (wet) intervals would result in a centripetal movement of the nearshore (offshore) particles, which facilitates the deposition of larger (finer) grains in the lake center (Xiao et al., 2009). However, field investigation indicated that the perennial inflow and outflow streams could maintain the lake level constant throughout the year (Huang et al., 2025). These results indicate that the sorting effects of the post-depositional process might have little influence on the grain size composition. Intuitively, during periods of increased monsoonal precipitation, the river discharge will enhance and the transporting dynamic will largely improve, which leads to greater erosion and more deposition of coarser particles into the lake. Furthermore, for Lake MangCo, the close proximity of the lake's inlet and outlet would facilitate the runoff of fine particulate matter in the suspended state in the water

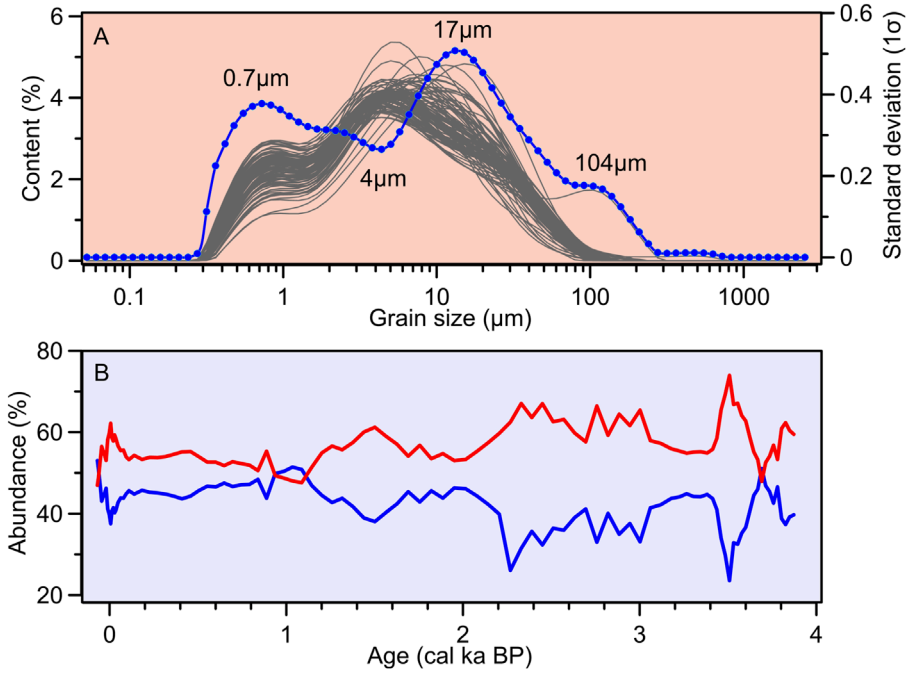

FIGURE 4
Grain size analysis results in Lake MangCo. **(A)** Grain size distribution curve of the sediment cores (gray lines) and the grain size vs. standard deviation diagram (blue dotted line); **(B)** variation in sensitive components (SC1, blue line; SC2, red line) over the late Holocene.

flow without settling within the lake. Therefore, layers with larger grain sizes in Lake MangCo sediments (i.e., higher SC2 content) should indicate wetter conditions and stronger ISM.

To validate the climatic interpretation of grain size in Lake MangCo, we compared the SC2 content with the regional instrumental precipitation history from the Zuogong meteorological station and the tree ring stable oxygen isotope values ($\delta^{18}O$) (An et al., 2013). The general decreasing trend in precipitation over the past 60 years corresponds with the decrease in the SC2 content (Figure 5A). Particularly, the significant precipitation reduction in 1970 results in very low SC2 abundance. These results consolidate SC2 content as a proxy of erosion intensity and monsoonal precipitation strength. On a longer timescale, the tree ring $\delta^{18}O$ values from the southeastern Tibetan Plateau record the changes in relative humidity, where much negative bias in $\delta^{18}O$ indicates a humid environment (Figure 5B). The overall negative correlation between SC2 content and the tree ring $\delta^{18}O$ from the Batang–Litang Plateau further confirms that the SC2 changes could reflect the regional hydroclimate and, in turn, the ISM strength.

4.2 Millennial-scale monsoon variation and its forcing mechanisms

On a millennial timescale, the higher SC2 content, likely before 2.0 cal ka BP, indicates stronger catchment erosion during the first half of the late Holocene, which was related to enhanced ISM at that time. However, the relatively low SC2 factions thereafter indicate subdued monsoonal precipitation compared to the earlier period. Such an ISM evolution pattern characterized by a gradual decrease during the late Holocene is in accordance with the regional paleoclimate records. For example, the general decrease in median grain size and magnetic susceptibility from Lake Ruogen Co during 4.2–1.3 cal ka BP indicated that the ISM gradually weakened during the middle-to-late Holocene transition (Ming et al., 2020; Figure 6B). The *Tsuga* pollen percentage from Lake Tiancai and Lake Lugu continuously decreased, which indicates a tendency of weaker ISM since the late Holocene (Xiao et al., 2014). The long-term decreasing exogenous material input, as reflected by the decreasing trend of Ti/Ca and Fe/Ca ratios since 4.0 cal ka BP in Lake Qionghai, also indicated that the ISM has persistently weakened from middle-to-late Holocene (Sun et al., 2023). The positive bias in $\delta^{13}C_{cellous}$ values from Hongyuan Bog (Hong et al., 2003), $\delta^{18}O_{stalagmite}$ values from Dongge Cave (Dykoski et al., 2005), and in δD_{alkane} values from the Bay of Bengal (Contreras-Rosales et al., 2014) after 4.0 cal ka BP have all indicated a late Holocene weak ISM environment. It can be observed that all these records broadly follow the trend of NHSI (Laskar et al., 2011; Figure 6F). The synchronicity between paleoclimatic records and the orbital NHSI intensity supports the hypothesis that paleo-ISM intensity has been primarily controlled by solar insolation on a millennial timescale (Wang et al., 2005). The gradually decreasing NHSI since the late Holocene resulted in a reduced thermal contrast between the tropical ocean and the Asian continent and hampered the northward migration of the Intertropical Convergence Zone (ITCZ) (Haug et al., 2001). This led to a decrease in the monsoonal precipitation in Lake MangCo since 4.0 cal ka BP.

However, although the SC2 content remained relatively low after 2.0 cal ka BP compared to the earlier period of the late Holocene, a slight increasing trend, particularly since 1.1 cal ka BP, can be

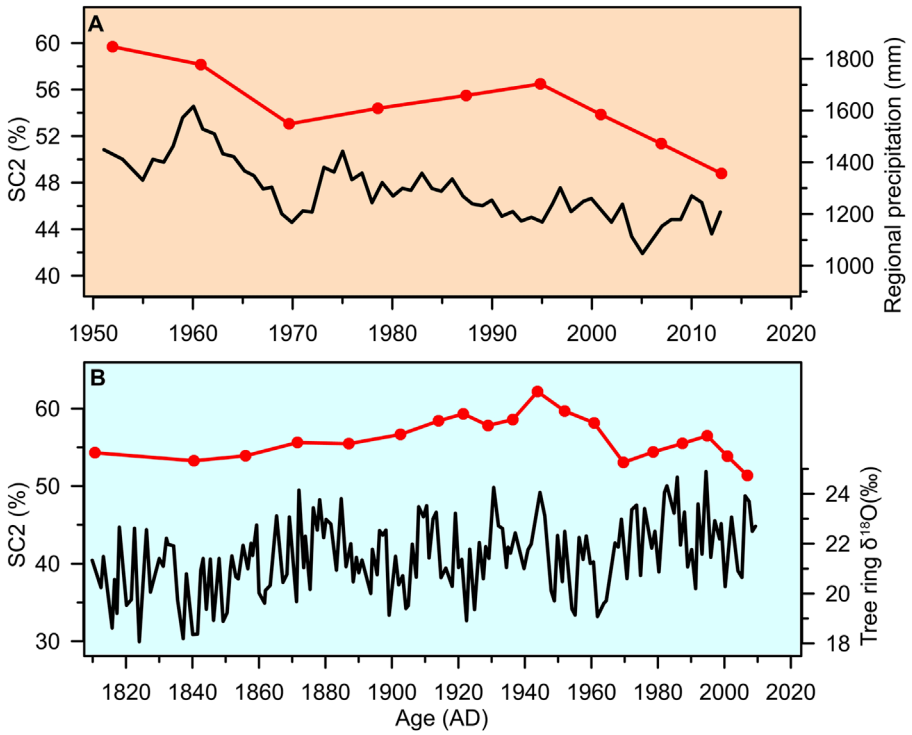

FIGURE 5
Comparison between the SC2 content (4–79 μm) in Lake MangCo and the regional precipitation over the past 60 years **(A)** and the tree ring $\delta^{18}O$ values from the Batang–Litang Plateau over the past 200 years (An et al., 2013, **(B)**).

identified (Figure 5A). Similar re-strengthening in ISM intensity since the last millennium has also been observed in previous paleoclimate studies. $\delta^{13}C_{org}$ and median grain size from Lake Ruogen Co showed that the regional climate became much wetter since 1.3 cal ka BP (Ming et al., 2020; Figure 5B). The dramatic increase in the small grain size content and Ti counts for the past 1,000 years indicated an abrupt increase in the lake level caused by an increase in monsoonal precipitation (Zhang et al., 2017). The planktonic foraminifer (*G. bulloides*) abundance in marine sediments from the west Arabian Sea increased since 1.5 cal ka BP, which was related to the enhancement of upwelling reflecting stronger monsoon wind (Anderson et al., 2010; Figure 5E). In the Qunf Cave, stalagmite deposition reinitiated at 1.4 cal ka BP and was followed by continuous depletion, which also indicates a strengthening tendency of ISM during the past millennium (Fleitmann et al., 2003). Some paleoclimate studies have even observed a much earlier onset of stronger ISM that started at ~ 2.0 cal ka BP (Cheng et al., 2016; Wang J. et al., 2024). Such late Holocene anomaly has been linked to the "2-kyr shift" based on the significant negative shift in $\delta^{18}O_{stalagmite}$ after 2.0 cal ka BP (Cheng et al., 2016). The paradoxical timing of the onset of climate shifts recorded in different materials might be attributed to the varying sensitivity of various proxies to climate changes or to dating uncertainties; however, it is unquestionable that the ISM has strengthened at least since the last one millennium.

Clearly, the re-enhancement of ISM at the end of the late Holocene contrasts with the attenuation of the NHSI. Cheng et al. (2016) proposed that the progressive increase in the rate of AMOC over the past 2 kyr might be the origin of the "2-kyr shift." The increase in the AMOC contributes to the meridional development of Hadley circulation, which generates the northward migration or the expanded latitudinal range of ITCZ and, finally, causes wetter conditions in the north tropical and subtropical areas, including the ISM-affected domains. Several studies show constant and slight increase in the AMOC for the past few millennia (Kissel et al., 2013); however, multiple global climate model simulation results indicate no consistent trend in overall AMOC strength since the middle Holocene (Jiang Z. et al., 2023). These results might indicate that other internal factors might have influenced the late Holocene climate shift.

The tropical temperature could play an important role in hydroclimate changes in Asian monsoon regions (Zhang et al., 2017). The Clausius–Clapeyron equation states that a 7% increase in integrated water vapor for every degree Celsius results in a 2%–3% increase in precipitation, subject to energetic constraints (Chen et al., 2019). This means a slight temperature increase in tropical regions would significantly increase the atmospheric moisture-holding capability. Therefore, following the monsoonal circulation, the water-enriched air streams under higher temperature conditions would provide much more precipitation to the inland. During the late Holocene, the generally warming trend in the tropics, likely after 2.0 cal ka BP, is associated with enhanced ISM precipitation (Marcott et al., 2013; Figure 6F). Although there are divergences in the magnitude and duration of tropical temperature changes and precipitation fluctuations, their overall similarity indicates that the tropical temperature anomalies could be an alternative explanation

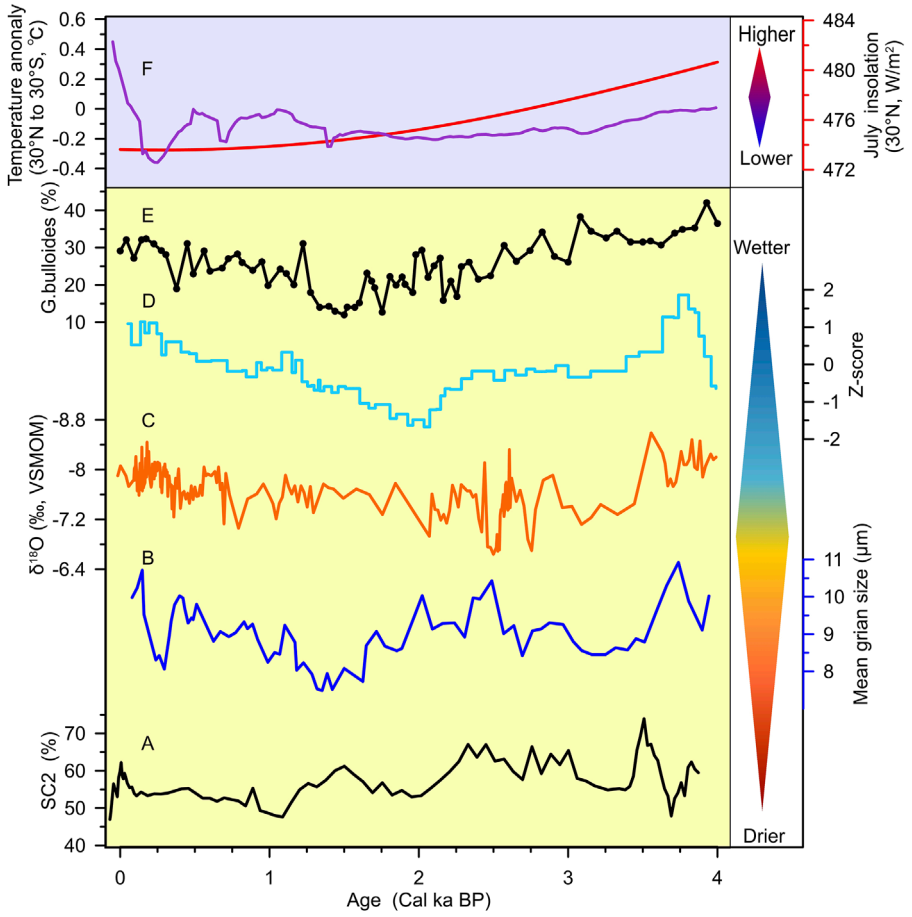

FIGURE 6
Comparison between the SC2 content (4–79 μm) in Lake MangCo **(A)** and the regional paleoclimatic records **(B–E)** including the mean grain size in Lake Ruogen Co **(B)** (Ming et al., 2020), $\delta^{18}O_{stalagmite}$ values in the Dongge Cave **(C)** (Dykoski et al., 2005), Z-score of stacked moisture record (comprising a*, Rb/Sr, CIA, Ki, and the <2 μm content) in the Mirui section **(D)** (Wang H. et al., 2024), and the abundance of planktic foraminifer, *Globigerina bulloides* in the Arabian Sea **(E)** (Anderson et al., 2010). The red and purple lines in panel **(F)** show the variations in 30°N July insolation and the compiled annual temperature changes between 30°N and 30°S (Marcott et al., 2013).

for the late Holocene climate shift. This phenomenon also provides insights into the effects of future global warming, indicating that increased rainfall would occur in the ISM-influenced regions in a warmer climate.

4.3 Centennial-scale monsoon fluctuation and its possible forcing

During the late Holocene, one of the most striking features in the SC2 content in Lake MangCo is the prominent deficits centered at ~ 3.2, 2.0, and 1.1 cal ka BP (Figure 7A). This result indicates that the ISM strongly weakened at that time and further illustrates significant centennial-scale ISM fluctuations over the past 4.0 ka BP. The ISM variations during MWP and LIA have been debated consistently (Sheng et al., 2015; Xu et al., 2017). The latest weak ISM event at ~ 1.1 cal ka BP likely corresponds to the dry conditions in ISM-influenced regions during MWP, which has been observed in several studies. For example, Poaceae rather than woody phytoliths constituted the greatest part of the phytolith assemblages in fluvial sediments during the MWP from southwestern China, which indicates a warm-dry climate during that time (Gu et al., 2020). The lowest broadleaf tree pollen in Lake Erhai (Xu et al., 2017) and lowest median grain size in Lake Lugu (Sheng et al., 2015) centered at approximately 1 cal ka BP indicates declined monsoonal rainfall during the MWP. The subdued catchment erosion during the MWP in Lake Qionghai has been recorded by lower Ti/Ca and Rb/Sr ratios between 1.0 and 0.6 cal ka BP, which also indicates a weak monsoon interval (Sun et al., 2023). Although human activities could complicate the interpretations of these climatic proxies in lake sediments because of slash-and-burn cultivations, the positive bias in $\delta^{18}O_{stalagmite}$ values at approximately ~1 cal ka BP in the Wanxiang Cave from southwestern China (Zhang et al., 2008), Hoti Cave from Oman (Fleitmann et al., 2007), and Mawmluh Cave from Northeastern India (Dutt et al., 2021) supports our inference of weakened ISM during the MWP. A slight increase in the SC2 content could also be observed in Lake MangCo at ~ 0.4–0.5 cal ka BP, which might indicate a similar wet condition during LIA,

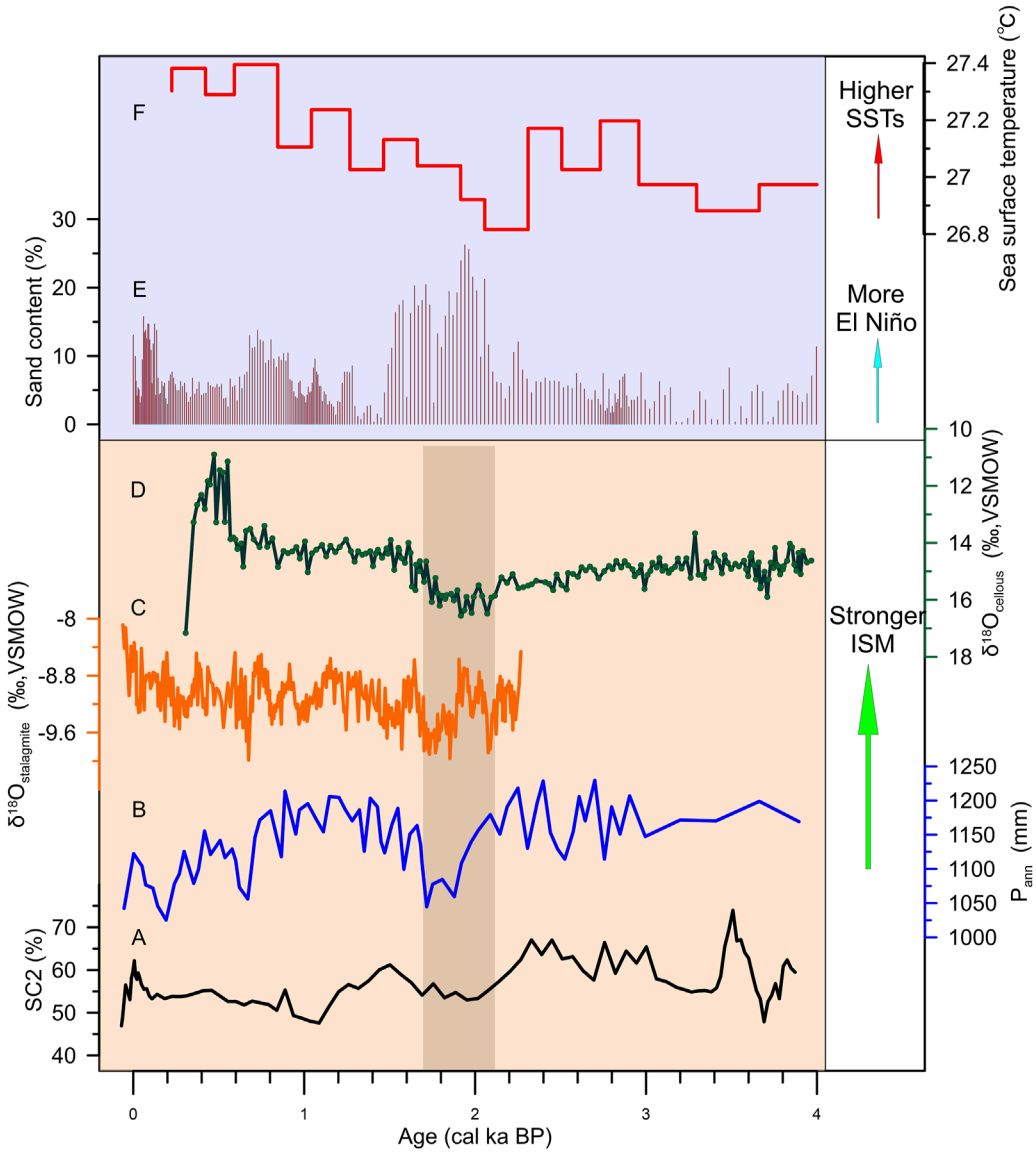

FIGURE 7
Centennial-scale ISM fluctuation **(A–D)** and the possible forcing **(E, F)**. **(A)** SC2 content (4–79 μm) in Lake MangCo (this study), **(B)** pollen-based mean annual precipitation from Tengchong Beihai wetland (Wang et al., 2020), **(C)** $\delta^{18}O_{stalagmite}$ values from the Shenqi Cave (Tan et al., 2018), **(D)** $\delta^{18}O$ values of α-cellulose in Dangxiong peatland (Wang J. et al., 2024), **(E)** sand content in Lake El Junco (Conroy et al., 2008), and **(F)** $U_{37}^{K'}$-based sea surface temperature reconstruction from the western Arabian Sea (Huguet et al., 2006).

as proposed in early studies (Sheng et al., 2015; Xu et al., 2017). However, for preciseness, we do not attribute this subtle change in SC2 at that time to the LIA event, and further studies are still needed.

The other two centennial ISM weakening events at ~ 3.2 and 2.0 cal ka BP are more obvious than that during MWP, and particularly, the later one has been called the "2.0-kyr dry event," characterized by significant positive $\delta^{18}O_{cellous}$ values in Dangxiong peat (Wang J. et al., 2024; Figure 7D). Mounts of palaeohydrological records have also captured the significant weak ISM event at ~ 2.0 cal ka BP. For example, the lowest median grain size in Lake Ruogen Co, occurred at approximately ~1.8 cal ka BP, indicated the weakest ISM intervals (Ming et al., 2020). The lowest Z-score values of stacked moisture proxies (including a*, Rb/Sr, CIA, Ki, and <2 μm content) in the Mirui loess section at ~ 2.0 cal ka BP also reflected drier conditions at that period (Wang H. et al., 2024; Figure 6D). The pollen-based precipitation from Tengchong Beihai wetland decreased significantly at ~ 1.8 cal ka BP, which visually demonstrated the weakening ISM event (Wang et al., 2020; Figure 7B). The much positive $\delta^{18}O_{stalagmite}$ values in the Shenqi Cave from southwestern China between 1.7 and 1.9 cal ka BP also indicate a significant centennial ISM weakening event (Tan et al., 2018; Figure 7C). On a broader spatial scale, this observation has also been supported by records from the Indian subcontinent and

Arabian sea sediments. The decrease in the abundance of cold-water foraminifera off the Oman margin occurred between 2.4 and 1.3 cal ka BP, which indicates a weakest Holocene upwelling interval that resulted from decreased summer monsoon wind (Anderson et al., 2010; Figure 6E). The speleothem record in the Qunf Cave exhibits a deposition hiatus between 2.7 and 1.4 cal ka BP, which also indicates a drier climate and weaker monsoon (Fleitmann et al., 2003). Although there are discrepancies between the initiation and duration of the drier conditions, as reflected in various records, a "2-kyr dry event" characterized by weakest ISM intensity could be identified.

It has been pointed out that the tropical ocean–atmosphere interactions have played crucial roles in influencing the decadal to centennial scale hydroclimate fluctuation in the monsoon-affected areas (Li et al., 2024; Wang et al., 2000). The El Niño-Southern Oscillation (ENSO) event has been recognized as the most important climate phenomenon among them, closely mirroring the latitudinal sea surface temperature gradient between the western and central-eastern Pacific basin (McPhaden et al., 2006). The ENSO-related response in the monsoon system is via the large-scale latitudinal migration in the Walker circulation over the tropical ocean (Kumar et al., 1999; Wang et al., 2000). During the warm phase of ENSO events (i.e., El Niño-like phase), the anomalous warmer waters in the central and eastern Pacific would result in an eastward shift of the ascending branch of the Walker circulation (Kumar et al., 1999; Wang et al., 2000). Consequently, an anomalous atmospheric subsidence would exist in the western Pacific region and penetrate the Indian subcontinent, which suppresses convection and precipitation in these regions. Notably, the strikingly weak ISM event at 2.0 cal ka BP in our study results coincides with lower sea surface temperatures in the western Pacific basin during 2.5–1.5 cal ka BP, corresponding to the El Niño-like phase (Linsley et al., 2010). The "2-kyr dry event" also agrees well with highest ENSO variability, as inferred by the sand content in the Lake El Junco sediment from Galápagos Islands between 2.1 and 1.8 cal ka BP (Conroy et al., 2008; Figure 7E). These consistencies suggest that the coupled feedbacks of large-scale tropical ocean–atmospheric interactions might modify the convective activities and, in turn, influence the ISM circulation.

Apart from the air–sea interactions in the Pacific basin, the tropical Indian Ocean SST anomaly also played a critical role in the short timescale ISM oscillations (Zhang et al., 2017). Warmer (lower) SSTs in the equatorial Indian Ocean, either resulted from the effect of solar insolation or the Pacific ENSO events, would increase the (decrease) convective process for the ISM above the ocean in a nonlinear way (Roxy et al., 2015), bringing more (less) moisture to the atmosphere. Monsoon winds would transport this enhanced (compressed) moisture signal across the Arabian Sea and the Bay of Bengal to South Asia and southwest China. Conspicuously, the prominent weak ISM events at ~ 3.2 and 2.0 cal ka BP correspond well with lower SSTs in the western Arabian Sea (Huguet et al., 2006; Figure 7F). The wetting trend after 2.0 cal ka BP in ISM-influenced areas is also likely related to the gradual warming in the tropical Indian Ocean basin (Huguet et al., 2006; Figure 7F). Therefore, we conclude that the centennial ISM fluctuations during the late Holocene might have been jointly influenced by the SST anomalies in tropical Pacific and Indian Ocean basins.

5 Conclusion

In this study, we investigated the late Holocene ISM variation based on the grain-size-sensitive components from Lake MangCo, located in the southeastern Tibetan Plateau. The grain size variation has been primarily controlled by regional hydrodynamic related to the monsoonal precipitation with coarser particles (higher SC2 content), indicating stronger ISM intensity. The relatively higher SC2 content, likely before 2.0 cal ka BP, and lower values thereafter reflect a general decreased ISM strength during the late Holocene. This phenomenon indicates that the changes in northern hemisphere summer insolation have dominantly controlled the ISM intensity. Our results also observed a slight increasing trend in ISM strength since 1.1 cal ka BP, which can be related to the reported "2.0-kyr-shift," and we propose that the warmer tropical temperature during the last few millenniums could be an alternative explanation. In addition, three low precipitation intervals centered at ~1.1, 2.0, and 3.2 cal ka BP corresponding well with centennial ISM weak events during the late Holocene such as the Medieval Warm Period and the "2.0-ka-dry-event." Our findings suggest that the tropical ocean–atmospheric interactions in the Pacific and Indian Ocean basins should be the predominant factor influencing the centennial ISM variability.

Data availability statement

The original contributions presented in the study are included in the article/Supplementary Material; further inquiries can be directed to the corresponding author.

Author contributions

DN: conceptualization, data curation, and writing–original draft. WS: conceptualization and writing–review and editing. DW: validation and writing–review and editing. LC: writing–review and editing. QJ: supervision and writing–review and editing.

Funding

The author(s) declare that financial support was received for the research, authorship, and/or publication of this article. This research was supported by the National Science Foundation of China (no. 42207512), the Nanjing Institute of Geography and Limnology of the Chinese Academy of Sciences (NIGLAS2022TJ01), and the Second Tibetan Plateau Scientific Expedition and Research Program (STEP) (no. 2019QZKK0202).

Acknowledgments

The authors would like to thank Xianqiang Meng and Zhenyu Ni for field assistance.

Conflict of interest

The authors declare that the research was conducted in the absence of any commercial or financial relationships that could be construed as a potential conflict of interest.

Generative AI statement

The author(s) declare that no Generative AI was used in the creation of this manuscript.

Publisher's note

Supplementary material

The Supplementary Material for this article can be found online at: https://www.frontiersin.org/articles/10.3389/feart.2025.1554436/full#supplementary-material

References

An, W., Liu, X., Leavitt, S. W., Xu, G., Zeng, X., Wang, W., et al. (2013). Relative humidity history on the Batang–Litang Plateau of western China since 1755 reconstructed from tree-ring $\delta^{18}O$ and δD. *Clim. Dyn.* 42, 2639–2654. doi:10.1007/s00382-013-1937-z

An, Z., Wu, G., Li, J., Sun, Y., Liu, Y., Zhou, W., et al. (2015). Global monsoon dynamics and climate change. *Annu. Rev. earth Planet. Sci.* 43, 29–77. doi:10.1146/annurev-earth-060313-054623

Anderson, D. M., Baulcomb, C. K., Duvivier, A. K., and Gupta, A. K. (2010). Indian summer monsoon during the last two millennia. *J. Quat. Sci.* 25, 911–917. doi:10.1002/jqs.1369

Appleby, P. G. (2001). "Chronostratigraphic techniques in recent sediments," in *Tracking environmental change using lake sediments: basin analysis, coring, and chronological techniques*. Editors W. M. Last, and J. P. Smol (Netherlands, Dordrecht: Springer), 171–203.

Bird, B. W., Lei, Y., Perello, M., Polissar, P. J., Yao, T., Finney, B., et al. (2017). Late-Holocene Indian summer monsoon variability revealed from a 3300-year-long lake sediment record from Nir'pa Co, southeastern Tibet. *Holocene* 27, 541–552. doi:10.1177/0959683616670220

Blaauw, M., and Christen, J. A. (2011). Flexible paleoclimate age-depth models using an autoregressive gamma process. *Bayesian Anal.* 457-474, 418. doi:10.1214/11-ba618

Chen, G., Norris, J., Neelin, J. D., Lu, J., Leung, L. R., and Sakaguchi, K. (2019). Thermodynamic and dynamic mechanisms for hydrological cycle intensification over the full probability distribution of precipitation events. *J. Atmos. Sci.* 76, 497–516. doi:10.1175/jas-d-18-0067.1

Chen, J., Chen, F., Feng, S., Huang, W., Liu, J., and Zhou, A. (2015). Hydroclimatic changes in China and surroundings during the medieval climate anomaly and little ice age: spatial patterns and possible mechanisms. *Quat. Sci. Rev.* 107, 98–111. doi:10.1016/j.quascirev.2014.10.012

Cheng, H., Edwards, R. L., Sinha, A., Spötl, C., Yi, L., Chen, S., et al. (2016). The Asian monsoon over the past 640,000 years and ice age terminations. *Nature* 534, 640–646. doi:10.1038/nature18591

Conroy, J. L., Overpeck, J. T., Cole, J. E., Shanahan, T. M., and Steinitz-Kannan, M. (2008). Holocene changes in eastern tropical Pacific climate inferred from a Galápagos lake sediment record. *Quat. Sci. Rev.* 27, 1166–1180. doi:10.1016/j.quascirev.2008.02.015

Contreras-Rosales, L. A., Jennerjahn, T., Tharammal, T., Meyer, V., Lückge, A., Paul, A., et al. (2014). Evolution of the Indian Summer Monsoon and terrestrial vegetation in the Bengal region during the past 18 ka. *Quat. Sci. Rev.* 102, 133–148. doi:10.1016/j.quascirev.2014.08.010

Cui, K., Wang, Y., Liu, X., Shen, J., and Wang, Y. (2022). Holocene variation in the Indian Summer Monsoon modulated by the tropical Indian Ocean sea-surface temperature mode. *CATENA* 215, 106302. doi:10.1016/j.catena.2022.106302

Dutt, S., Gupta, A. K., Cheng, H., Clemens, S. C., Singh, R. K., and Tewari, V. C. (2021). Indian summer monsoon variability in northeastern India during the last two millennia. *Quat. Int.* 571, 73–80. doi:10.1016/j.quaint.2020.10.021

Dykoski, C. A., Edwards, R. L., Cheng, H., Yuan, D., Cai, Y., Zhang, M., et al. (2005). A high-resolution, absolute-dated Holocene and deglacial Asian monsoon record from Dongge Cave, China. *Earth Planet. Sci. Lett.* 233, 71–86. doi:10.1016/j.epsl.2005.01.036

Fleitmann, D., Burns, S. J., Mangini, A., Mudelsee, M., Kramers, J., Villa, I., et al. (2007). Holocene ITCZ and Indian monsoon dynamics recorded in stalagmites from Oman and Yemen (Socotra). *Quat. Sci. Rev.* 26, 170–188. doi:10.1016/j.quascirev.2006.04.012

Fleitmann, D., Burns, S. J., Mudelsee, M., Neff, U., Kramers, J., Mangini, A., et al. (2003). Holocene forcing of the Indian monsoon recorded in a stalagmite from southern Oman. *Science* 300, 1737–1739. doi:10.1126/science.1083130

Gu, Y., Liu, H., Traoré, D. D., and Huang, C. (2020). ENSO-related droughts and ISM variations during the last millennium in tropical southwest China. *Clim. Dyn.* 54, 649–659. doi:10.1007/s00382-019-05019-1

Gupta, A. K., Das, M., and Anderson, D. M. (2005). Solar influence on the Indian summer monsoon during the Holocene. *Geophys. Res. Lett.* 32, L17703. doi:10.1029/2005gl022685

Hansen, G., and Stone, D. (2016). Assessing the observed impact of anthropogenic climate change. *Nat. Clim. Change* 6, 532–537. doi:10.1038/nclimate2896

Haug, G. H., Hughen, K. A., Sigman, D. M., Peterson, L. C., and Röhl, U. (2001). Southward migration of the intertropical convergence zone through the Holocene. *Science* 293, 1304–1308. doi:10.1126/science.1059725

Hong, Y. T., Hong, B., Lin, Q. H., Zhu, Y. X., Shibata, Y., Hirota, M., et al. (2003). Correlation between Indian ocean summer monsoon and north atlantic climate during the Holocene. *Earth Planet. Sci. Lett.* 211, 371–380. doi:10.1016/s0012-821x(03)00207-3

Huang, L., Zhu, L., Huang, Y., Wang, J., Ju, J., and Ma, Q. (2025). Hydroclimate variability in southeastern Tibetan Plateau since the late Quaternary: insights from hydrogen isotopes in sedimentary leaf waxes. *Catena* 248, 108569. doi:10.1016/j.catena.2024.108569

Huguet, C., Kim, J.-H., Sinninghe Damsté, J. S., and Schouten, S. (2006). Reconstruction of sea surface temperature variations in the Arabian Sea over the last 23 kyr using organic proxies (TEX86 and U37K′). *Paleoceanography* 21, PA3003. doi:10.1029/2005pa001215

Jiang, Y., Li, J., Wang, B., Yang, Y., and Zhu, Z. (2023a). Weakening of decadal variation of Northern Hemisphere land monsoon rainfall under global warming. *npj Clim. Atmos. Sci.* 6, 115. doi:10.1038/s41612-023-00441-z

Jiang, Z., Brierley, C. M., Bader, J., Braconnot, P., Erb, M., Hopcroft, P. O., et al. (2023b). No consistent simulated trends in the atlantic meridional overturning circulation for the past 6,000 years. *Geophys. Res. Lett.* 50, e2023GL103078. doi:10.1029/2023gl103078

Katzenberger, A., Schewe, J., Pongratz, J., and Levermann, A. (2021). Robust increase of Indian monsoon rainfall and its variability under future warming in CMIP6 models. *Earth Syst. Dyn.* 12, 367–386. doi:10.5194/esd-12-367-2021

Kissel, C., Van Toer, A., Laj, C., Cortijo, E., and Michel, E. (2013). Variations in the strength of the north atlantic bottom water during Holocene. *Earth Planet. Sci. Lett.* 369-370, 248–259. doi:10.1016/j.epsl.2013.03.042

Kumar, K. K., Rajagopalan, B., and Cane, M. A. (1999). On the weakening relationship between the Indian monsoon and ENSO. *Science* 284, 2156–2159. doi:10.1126/science.284.5423.2156

Laskar, J., Fienga, A., Gastineau, M., and Manche, H. J. A. (2011). La2010: a new orbital solution for the long-term motion of the Earth. *Radiocarbon* 532, A89. doi:10.1051/0004-6361/201116836

Last, W., and Smol, J. (2001). *Tracking environmental change using lake sediments: physical and geochemical methods*. Springer Science and Business Media.

Li, G., Yu, Z., Li, Y., Yang, C., Gu, H., Zhang, J., et al. (2024). Interaction mechanism of global multiple ocean-atmosphere coupled modes and their impacts on South and East Asian Monsoon: a review. *Glob. Planet. Change* 237, 104438. doi:10.1016/j.gloplacha.2024.104438

Linsley, B. K., Rosenthal, Y., and Oppo, D. W. (2010). Holocene evolution of the Indonesian throughflow and the western Pacific warm pool. *Nat. Geosci.* 3, 578–583. doi:10.1038/ngeo920

Liu, X., Vandenberghe, J., An, Z., Li, Y., Jin, Z., Dong, J., et al. (2016). Grain size of Lake Qinghai sediments: implications for riverine input and Holocene monsoon variability. *Palaeogeogr. Palaeoclimatol. Palaeoecol.* 449, 41–51. doi:10.1016/j.palaeo.2016.02.005

Marcott, S. A., Shakun, J. D., Clark, P. U., and Mix, A. C. (2013). A reconstruction of regional and global temperature for the past 11,300 years. *Science* 339, 1198–1201. doi:10.1126/science.1228026

McPhaden, M. J., Zebiak, S. E., and Glantz, M. H. (2006). ENSO as an integrating concept in Earth science. *Science* 314, 1740–1745. doi:10.1126/science.1132588

Ming, G., Zhou, W., Cheng, P., Wang, H., Xian, F., Fu, Y., et al. (2020). Lacustrine record from the eastern Tibetan Plateau associated with Asian summer monsoon changes over the past ~ 6 ka and its links with solar and ENSO activity. *Clim. Dyn.* 55, 1075–1086. doi:10.1007/s00382-020-05312-4

Ning, D., Xiao, X., Tang, S., Xu, Y., Kuai, X., Ge, Y., et al. (2024). Millennial to orbital scale Indian summer monsoon evolution inferred from grain size end-members in Tengchongbeihai wetland, southwestern China. *Quat. Sci. Rev.* 334, 108723. doi:10.1016/j.quascirev.2024.108723

Overpeck, J., Anderson, D., Trumbore, S., and Prell, W. (1996). The southwest Indian Monsoon over the last 18 000 years. *Clim. Dyn.* 12, 213–225. doi:10.1007/s003820050104

Prasad, S., Anoop, A., Riedel, N., Sarkar, S., Menzel, P., Basavaiah, N., et al. (2014). Prolonged monsoon droughts and links to Indo-Pacific warm pool: a Holocene record from Lonar Lake, central India. *Earth Planet. Sci. Lett.* 391, 171–182. doi:10.1016/j.epsl.2014.01.043

Reimer, P. J., Austin, W. E. N., Bard, E., Bayliss, A., Blackwell, P. G., Bronk Ramsey, C., et al. (2020). The IntCal20 northern hemisphere radiocarbon age calibration curve (0–55 cal kBP). *Radiocarbon* 62, 725–757. doi:10.1017/rdc.2020.41

Roxy, M. K., Ritika, K., Terray, P., Murtugudde, R., Ashok, K., and Goswami, B. N. (2015). Drying of Indian subcontinent by rapid Indian Ocean warming and a weakening land-sea thermal gradient. *Nat. Commun.* 6, 7423. doi:10.1038/ncomms8423

Sheng, E., Yu, K., Xu, H., Lan, J., Liu, B., and Che, S. (2015). Late Holocene Indian summer monsoon precipitation history at Lake Lugu, northwestern Yunnan Province, southwestern China. *Palaeogeogr. Palaeoclimatol. Palaeoecol.* 438, 24–33. doi:10.1016/j.palaeo.2015.07.026

Sun, H., Liu, X., Mao, X., Jia, W., and Herzschuh, U. (2023). Centennial-scale variability of the Indian Summer Monsoon during the middle to late Holocene and its links with ENSO activity. *Palaeogeogr. Palaeoclimatol. Palaeoecol.* 612, 111380. doi:10.1016/j.palaeo.2022.111380

Sun, Y., Gao, S., and Li, J. (2003). Preliminary analysis of grain-size populations with environmentally sensitive terrigenous components in marginal sea setting. *Chin. Sci. Bull.* 48, 184–187. doi:10.1360/03tb9038

Tan, L., Cai, Y., Cheng, H., Edwards, L. R., Lan, J., Zhang, H., et al. (2018). High resolution monsoon precipitation changes on southeastern Tibetan Plateau over the past 2300 years. *Quat. Sci. Rev.* 195, 122–132. doi:10.1016/j.quascirev.2018.07.021

Tiwari, M., Nagoji, S. S., and Ganeshram, R. S. (2015). Multi-centennial scale SST and Indian summer monsoon precipitation variability since the mid-Holocene and its nonlinear response to solar activity. *Holocene* 25, 1415–1424. doi:10.1177/0959683615585840

Verma, S., Bhatla, R., Shahi, N. K., and Mall, R. K. (2022). Regional modulating behavior of Indian summer monsoon rainfall in context of spatio-temporal variation of drought and flood events. *Atmos. Res.* 274, 106201. doi:10.1016/j.atmosres.2022.106201

Wang, B., Wu, R., and Fu, X. (2000). Pacific–East asian teleconnection: how does ENSO affect east asian climate? *J. Clim.* 13, 1517–1536. doi:10.1175/1520-0442(2000)013<1517:peathd>2.0.co;2

Wang, H., Yang, J., Gao, F., Wang, S., Wang, Z., Qu, W., et al. (2024a). Middle to late Holocene climate change in the monsoon-dominated southeastern Tibetan Plateau and its relationship with human activity. *Palaeogeogr. Palaeoclimatol. Palaeoecol.* 645, 112209. doi:10.1016/j.palaeo.2024.112209

Wang, J., Peng, H., Uchida, M., Zhao, H., Ding, H., Yao, H., et al. (2024b). Holocene dynamics of the Indian summer monsoon inferred from a high-resolution peat α-cellulose $\delta^{18}O$ record on the Tibetan Plateau. *Quat. Sci. Rev.* 342, 108913. doi:10.1016/j.quascirev.2024.108913

Wang, Y., Cheng, H., Edwards, R. L., He, Y., Kong, X., An, Z., et al. (2005). The Holocene asian monsoon: links to solar changes and north atlantic climate. *Science* 308, 854–857. doi:10.1126/science.1106296

Wang, Y., Shen, J., Wang, Y., Liu, X., Cao, X., and Herzschuh, U. (2020). Abrupt mid-Holocene decline in the Indian Summer Monsoon caused by tropical Indian Ocean cooling. *Clim. Dyn.* 55, 1961–1977. doi:10.1007/s00382-020-05363-7

Xiao, J., Chang, Z., Si, B., Qin, X., Itoh, S., and Lomtatidze, Z. (2009). Partitioning of the grain-size components of Dali Lake core sediments: evidence for lake-level changes during the Holocene. *J. Paleolimnol.* 42, 249–260. doi:10.1007/s10933-008-9274-7

Xiao, X., Haberle, S. G., Shen, J., Yang, X., Han, Y., Zhang, E., et al. (2014). Latest Pleistocene and Holocene vegetation and climate history inferred from an alpine lacustrine record, northwestern Yunnan Province, southwestern China. *Quat. Sci. Rev.* 86, 35–48. doi:10.1016/j.quascirev.2013.12.023

Xu, H., Zhou, X., Lan, J., Liu, B., Sheng, E., Yu, K., et al. (2017). Late Holocene Indian summer monsoon variations recorded at Lake Erhai, southwestern China. *Quat. Res.* 83, 307–314. doi:10.1016/j.yqres.2014.12.004

Zhang, E., Zhao, C., Xue, B., Liu, Z., Yu, Z., Chen, R., et al. (2017). Millennial-scale hydroclimate variations in southwest China linked to tropical Indian Ocean since the Last Glacial Maximum. *Geology* 45, 435–438. doi:10.1130/g38309.1

Zhang, P., Cheng, H., Edwards, R. L., Chen, F., Wang, Y., Yang, X., et al. (2008). A test of climate, Sun, and culture relationships from an 1810-year Chinese cave record. *Science* 322, 940–942. doi:10.1126/science.1163965

Zhang, X., Jin, L., and Jia, W. (2016). Centennial-scale teleconnection between North Atlantic sea surface temperatures and the Indian summer monsoon during the Holocene. *Clim. Dyn.* 46, 3323–3336. doi:10.1007/s00382-015-2771-2